Self-Standing, Collector-Free Maricite $NaFePO_4$/Carbon Nanofiber Cathode Endowed with Increasing Electrochemical Activity

Xinyang Liu-Théato, Sylvio Indris,* Weibo Hua, Hang Li, Michael Knapp, Georgian Melinte, and Helmut Ehrenberg

ABSTRACT: A new electrode design for sodium ion batteries with a self standing, collector free, binder free maricite $NaFePO_4$/carbon nanofiber hybrid cathode is successfully realized via electrospinning. An increasing capacity is observed in the initial cycles, and finally, the electrode reached a capacity of 108 mAh g^{-1} at a 0.1 C rate after 200 cycles. In comparison, a slurry based $NaFePO_4$ electrode yields a capacity of only around 20 mAh g^{-1}. An overall improved electrochemical performance was obtained in the hybrid cathode compared to pure slurry based $NaFePO_4$ electrode and pure carbon nanofibers. A comprehensive study of the morphology, structure, and electrochemical performance of the hybrid electrode is conducted. Mössbauer spectra show an increasing Fe^{3+} content from 43.2% in the first charged state to 63.0% in the charged state after 100 cycles, demonstrating an activating process of maricite $NaFePO_4$ upon extensive charge−discharge cycling. This work has explored a direct electrospun self standing maricite $NaFePO_4$ electrode and its feasibility and mechanism as a cathode material in sodium ion batteries.

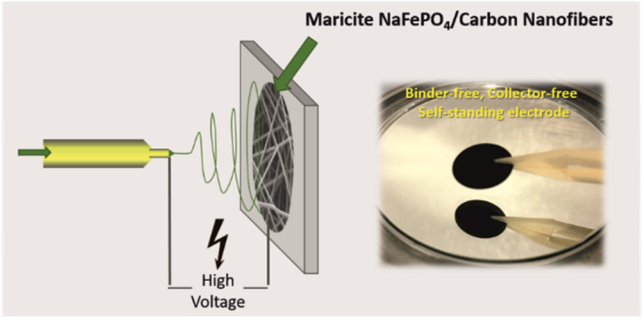

1. INTRODUCTION

Sodium ion batteries (SIBs) have received increasing attention from researchers as a result of the wide availability and low cost of sodium compared to lithium.[1] SIBs show great potential, especially in large scale stationary energy storage systems, where the requirement of abundance and low cost of raw materials is yet to be fulfilled.[2] Although sharing similar chemical properties and electrochemical reactions with Li^+, Na^+ possesses a higher mass and larger ionic radius.[1,3] Thus, a stable structure of a Na^+ host material that can both withstand the volume change for long cycle life and deliver a reasonable high rate capability is in high demand.[4] Inspired by the success of $LiFePO_4$ in the case of Li batteries, iron based phosphates are in focus because they show good structural stability during cycling with only a 6.8% volume reduction from $LiFePO_4$ to $FePO_4$.[5] Moreover, in comparison to other candidates, the use of iron also avoids environmentally unfriendly metals, such as cobalt, and toxic elements, such as vanadium.[6] Furthermore, among iron based cathode materials, $NaFePO_4$ offers the highest theoretical capacity up to 154 mAh g^{-1} and a decent working voltage range.[7,8]

Triphylite and maricite structures are two crystal structures of $NaFePO_4$, of which the triphylite structure is not thermodynamically stable and the maricite structure is inhibited from applications as a result of its electrochemically inactive nature.[9−11] However, $LiFePO_4$ was also once believed to be incapable of performing as a cathode material as a result of its low electrical conductivity until approaches of particle size reduction and coating with conductive materials were used for its commercialization.[12] Consequently, also for maricite $NaFePO_4$, attempts, such as particle downsizing and carbon addition, have been undertaken in recent studies to successfully deliver high capacities of maricite $NaFePO_4$.[13] For example, Kim et al. proved a full deintercalation of Na^+ ions from nanosized maricite $NaFePO_4$.[14] Rahman et al. synthesized a hybrid material of $NaFePO_4$/C/graphene by ball milling with the addition of graphene to achieve an improved cycle performance with a capacity of 142 mAh g^{-1} at 0.1 C after 300 cycles.[15] Fan's group has used electrospinning for nanoparticle synthesis, realizing an embedding of $NaFePO_4$ nanodots (≈1.6 nm) in N doped carbon fibers to obtain a high reversible capacity of 145 mAh g^{-1} at 0.2 C.[16] Via electrospinning, Fan's group has realized a binder free electrode without the procedure of slurry making and coating, which were necessary in other reported work. However, the aluminum foil was unavoidably included during the whole procedure. The question has been raised: is it possible to

synthesize a binder free, collector free, self standing $NaFePO_4$ electrode material? Moreover, a high surface area of the electrode material can be generated from the nanoparticles and carbon content, which may unavoidably result in a surface storage of charges contributing to the overall capacity.[17] This capacitive charge storage contribution was often neglected in such nanostructured maricite $NaFePO_4$ electrodes.

Electrospinning is usually used as one method for the synthesis of nanoparticles for a binder free electrode.[18,19] In general, there are two different approaches: (i) nanoparticle synthesis: starting materials are first dissolved in polymer solutions for electrospinning (aqueous or organic solvent), and the crystalline nanoparticles are synthesized during subsequent calcination along with the decomposition of polymer fiber;[20,21] (ii) post carbon nanofiber coating: nanoparticles of the electrodes are directly dispersed in the carbon source polymer solutions, and the carbon nanofiber coated composites are formed during the high temperature carbonization.[22,23] Bach tin et al. improved the electrical conductivity of $LiFePO_4$ and its cycle stability via a direct electrospinning from the hybrid solution of $LiFePO_4$ and polyacrylonitrile (PAN), resulting in a carbon decorated $LiFePO_4$ after carbonization of PAN.[24] However, a corresponding electrode fabrication/design from the electrospinning of maricite $NaFePO_4$ product has, to our knowledge, not yet been reported. In comparison to the reported electrospinning methods from starting materials of $NaFePO_4$, this direct carbon coating approach is less time consuming and more straightforward. In this way, not only can improved electrical conductivity be introduced, but the carbon nanofiber network can also function as the current collector, realizing a self standing and collector free electrode material, which can be used in flexible, soft, and wearable batteries.

Herein, we synthesized for the first time a collector free, self standing $NaFePO_4$/carbon nanofiber ($NaFePO_4$/CNF) elec trode via electrospinning of ball milled $NaFePO_4$ and PAN/*N*,*N* dimethylformamid (DMF) solution. A comprehensive investigation of the electrode morphology, structure, and electrochemical performance before and after cycling is carried out. The study of such a composite electrode material will enlighten the knowledge on (1) the Na^+ ion transfer mechanism in carbon containing cathode material, (2) the capacitive contribution of the carbon content and nanoma terials in SIBs, and (3) potentials of such self standing, collector free, binder free electrodes in the field of energy storage systems.

2. EXPERIMENTAL SECTION

2.1. Preparation of Self-Standing $NaFePO_4$/CNF. Na_2CO_3 (99.95%, Acros), $FeC_2O_4{\cdot}2H_2O$ (99%, Alfa Aesar), and $NH_4H_2PO_4$ (99.99%, Sigma Aldrich) with the molar ratio of 0.5:1:1 were used as starting materials for the synthesis of $NaFePO_4$ nanoparticles as described before by Kim et al.[14] All starting materials were ground and then loaded into the ball milling container with ZrO_2 milling balls. The mixed precursors were milled for more than 24 h at 500 rpm and then calcined at 350 °C under an argon atmosphere for 5 h before being re ground and pressed into pellets. The pellets underwent a second calcination at 600 °C under argon for 10 h and then were ground for further use. Next, the ground $NaFePO_4$ nanoparticles were dispersed in a PAN/DMF solution under strong stirring overnight with a mass ratio of $NaFePO_4$/PAN of 1:2. This composite solution was then loaded into a 1 mL syringe attached to an assembled injecting needle with a diameter of 0.8 mm. A climate controlled electrospinning apparatus (EC CLI, IME Technologies) was used with the temperature and humidity set to 25 °C and 20%, respectively. A high voltage of 13−16 kV was applied between the needle tip and the collector covered by a sheet of aluminum foil. The flowing rate of solution was 0.5 mL h^{-1}, and the tip to collector distance was 15 cm. In total, the 1 mL solution was spun 2 times into one fiber mat. The fiber mat was then vacuum dried and stabilized in air with heating steps to the highest temperature of 280 °C before being carbonized under argon at 600 °C for 1 h.

2.2. Material Characterization. The morphology of electrodes was observed with Merlin field emission scanning electron microscopy (FE SEM, Carl Zeiss SMT AG). Energy dispersive X ray spectrosco py (EDX) was performed to analyze the elemental compositions (Bruker Quantax, 400 SDD). X ray diffraction (XRD) measurements were carried out on a STOE STADI P X ray powder diffractometer with a Mythen 1K detector and Mo $K\alpha_1$ radiation (λ = 0.7093 Å). Thermogravimetric analysis (TGA) was performed to determine the content of carbon and active material in the composite electrode. It was carried out on a STA 449 C Jupiter instrument (NETZSCH) with a heating rate of 10 K min^{-1} up to 1200 °C in an oxygen atmosphere. The Brunauer−Emmett−Teller (BET) specific surface area was detected via the nitrogen adsorption method (Gemini VII 2390, Micromeritics). *In situ* high temperature XRD (HT XRD) was carried out at synchrotron at Paul Scherer Institute (PSI), Villigen, Switzerland. $NaFePO_4$ powders were heated in air with a heating rate of 20 °C min^{-1} from 90 to 400 °C and then cooled to 90 °C. During heating and cooling, 53 XRD patterns were recorded. The wavelength (λ) was 0.5106 Å, and a MYTHEN II detector was used.

2.3. *Ex Situ* Characterization. Mössbauer spectroscopy was performed at room temperature with a constant acceleration spectrometer in transmission mode and a $^{57}Fe(Rh)$ source. All isomer shifts are given relative to that of α Fe metal. The cells were charged to 4.5 V and discharged to 1.5 V in the initial cycle and the 100th cycle, separately. The cells were disassembled afterward, and cathode materials were washed with dimethyl carbonate (DMC), dried at 60 °C for 12 h, and then sealed in polyethylene/aluminum bags in an argon filled glovebox (O_2 and H_2O < 0.1 ppm). Raman spectroscopy was performed on a LabRam Evolution HR instrument (HORIBA Jobin Yvon) applying a 532 nm wavelength laser. Each spectrum was taken as the average of three 45 s accumulations. For the transmission electron microscopy (TEM) measurements, the samples were prepared inside a glovebox and transferred to the microscope without exposure to air using a vacuum transfer holder. The dry powder was directly dispersed on the TEM holey carbon membrane without the use of solvents. The measurements were performed using a Themis300 electron microscope working at 300 kV and equipped with a DCOR probe corrector and a Super X EDX detector. High angle annular dark field (HAADF) and scanning transmission electron microscopy−energy dispersive X ray spectros copy (STEM−EDX) elemental mapping were performed to elucidate the morphology of the carbon fibers.

2.4. Electrochemical Performance. The electrochemical per formance was studied in coin cells (CR2032) with sodium metal as the counter/reference electrode, glass fiber (Whatman, GF/D) as the separator, and 0.8 M $NaClO_4$ in ethylene carbonate (EC)/diethyl carbonate (DEC) (1:1, w/w) as the electrolyte. The electrospun self standing electrodes were punched into the right size (⌀ = 12 mm) and directly assembled in the coin cells without any additional current collector. Galvanostatic cycling, cyclic voltammetry (CV), and electrochemical impedance spectroscopy (EIS) were carried out on a multichannel potentiostat (VMP3, Bio Logic). The voltage ranges of galvanostatic cycling and CV tests are 4.5−1.5 V versus Na^+/Na. The galvanostatic mode was a constant current−constant voltage (CC−CV) charging mode at 0.1 C, with the voltage of 4.5 V holding for 5 h with a current limit of 0.05 C. The calculation of the specific capacity of $NaFePO_4$/CNF is based on the mass of $NaFePO_4$. EIS tests were carried out at the charged state (4.5 V) and discharged state (1.5 V) with an alternating current signal of a 5 mV amplitude and frequencies ranging from 1 MHz to 0.01 Hz.

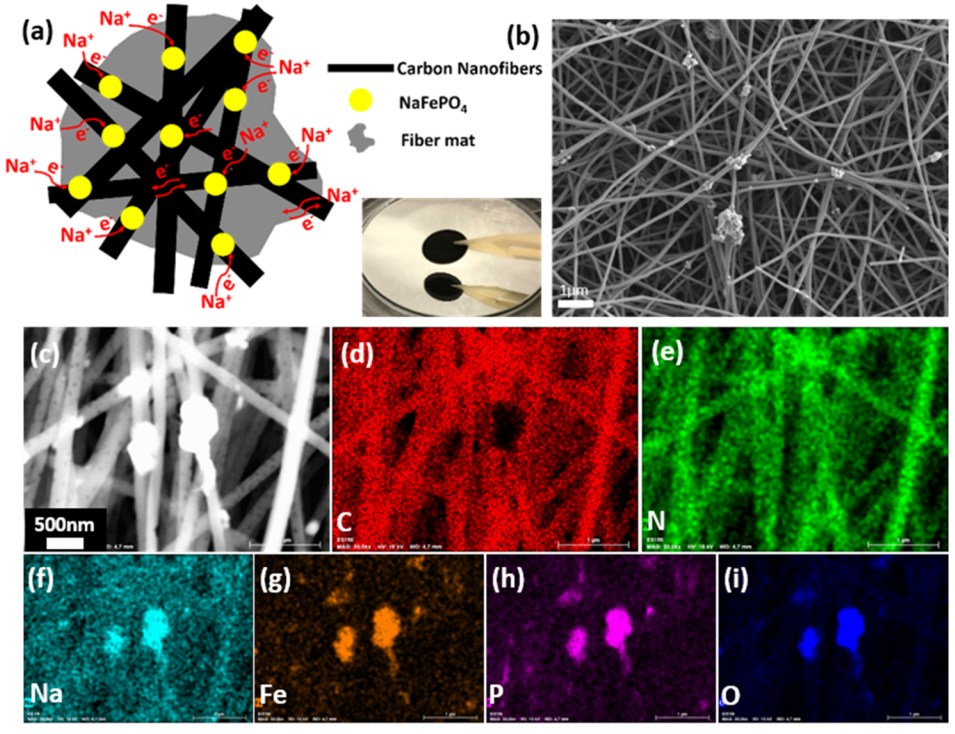

Figure 1. (a) Schematic illustration of the possible Na^+ ion pathways in the carbon nanofiber matrix with an optical photograph of the self standing electrode, (b) SEM images of the electrospun $NaFePO_4$/CNF electrodes, and (c–i) EDX mappings of elements: (d) carbon (C), (e) nitrogen (N), (f) sodium (Na), (g) iron (Fe), (h) phosphorus (P), and (i) oxygen (O).

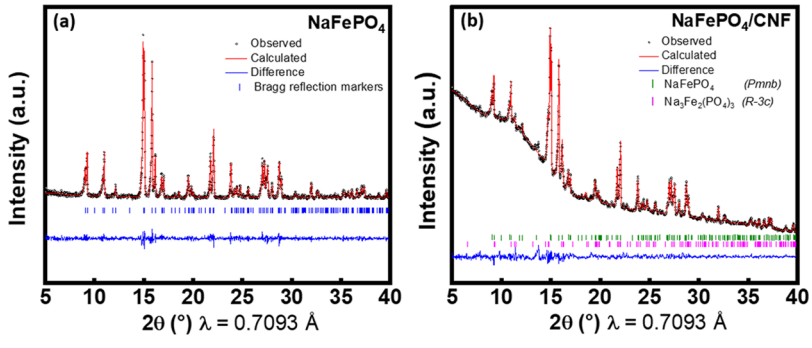

Figure 2. Rietveld refinement on XRD patterns of (a) as prepared $NaFePO_4$ powder and (b) $NaFePO_4$/CNF cathodes, with λ = 0.70932 Å.

3. RESULTS AND DISCUSSION

3.1. Material Characterization. Maricite $NaFePO_4$ nanoparticles were first prepared via mechanical ball milling and then dispersed in the polymer solution under strong stirring for further electrospinning. Under high voltages, the nanofibers were collected on an aluminum foil and then treated with a two step heating procedure, resulting in a flexible, black colored, self standing mat, which can be cut into electrodes and directly assembled in coin cells without further handling. It is generally known that maricite $NaFePO_4$ is electrochemically inactive as a result of the lack of pathways for Na^+ ion transport. By integration of maricite $NaFePO_4$ particles onto carbon nanofiber (CNF) mats, the high porosity of the fiber network can enhance the contact between the electrolyte and active material, as proposed in Figure 1a. Moreover, the carbon content can improve the electrical conductivity, facilitating a better electrochemical performance of such a hybrid electrode. A 30 wt % weight percentage of $NaFePO_4$ within the hybrid electrode was determined by TGA measurement (see Figure S1 of the Supporting Information). The morphology of the obtained self standing electrode is shown in Figure 1b, with the $NaFePO_4$ particles dispersed homogeneously in the carbon nanofibers. Clusters of the active material as a result of agglomeration can also be observed. The EDX results in panels c–i of Figure 1 show that the active material particles consist of Na, Fe, P, and O and are embedded in the nanofibers that consist of C and N. Noteworthy, the traces of nitrogen are the residue from the low temperature carbonization process of PAN.[25]

The structures of $NaFePO_4$ and $NaFePO_4$/CNF electrodes were also investigated by XRD. As shown in Figure 2a, a phase pure maricite structure of $NaFePO_4$ indexed on the basis of a *Pmnb* orthorhombic model was obtained. With a Rietveld refinement, the lattice parameters of $NaFePO_4$ were determined as a = 6.8659(2) Å, b = 8.9761(2) Å, and c = 5.0412(2) Å, matching well with values reported in the literature.[26−28] As shown in Figure 2b, the presence of carbon nanofibers in the composites with CNF introduced an obvious amorphous phase, underlying the reflections from crystalline

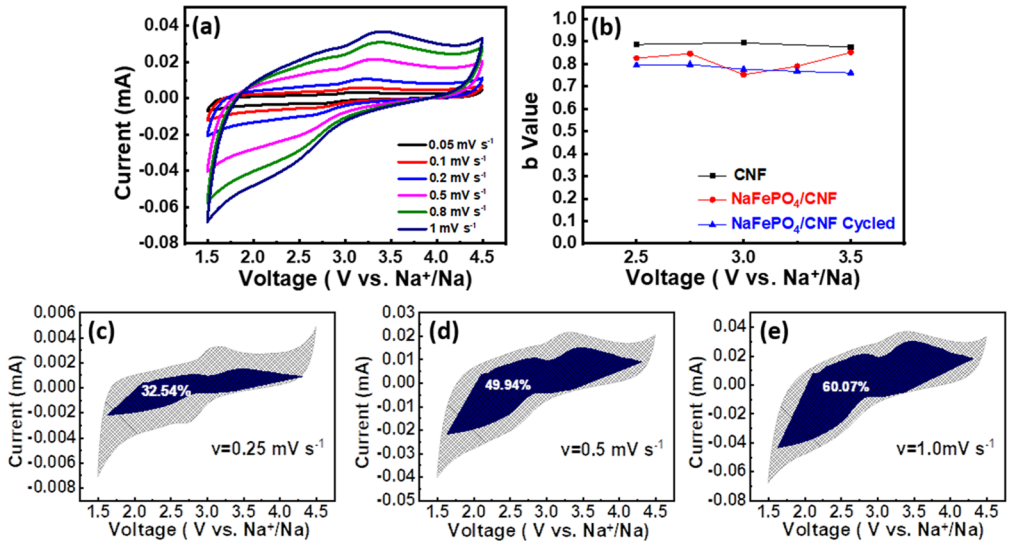

Figure 3. (a) CV curves at various scan rates from 0.05 to 1 mV s^{-1}, (b) *b* values at different potentials of pure CNF, pristine $NaFePO_4$/CNF electrodes, and cycled $NaFePO_4$/CNF electrodes, and the contribution of capacitive controlled (blue) and diffusion controlled (gray) capacities to the total capacity for $NaFePO_4$/CNF electrodes at different scan rates: (c) 0.25 mV s^{-1}, (d) 0.5 mV s^{-1}, and (e) 1.0 mV s^{-1}.

$NaFePO_4$. Some new reflections appeared for the $NaFePO_4$/CNF electrodes at low angles (5−7° and 11−14°, respectively), which may refer to some impurity phases. According to the HT XRD of $NaFePO_4$ in air, some new reflections start to show up at around 230 °C (Figure S2 of the Supporting Information). To gain a deeper knowledge of these new reflections, Rietveld refinement was conducted on the HT XRD patterns. Accordingly, a new NASICON phase $Na_3Fe_2(PO_4)_3$ (space group *R*3*c*) was detected (Figure S3a of the Supporting Information).[29] Lattice parameters of *a* and *c* were determined as 8.7317(2) and 21.6663(2) Å, respectively. Partial oxidization of $NaFePO_4$ was proposed to occur during the heating under air. The lattice parameters were determined as a function of the temperature (Figure S3b of the Supporting Information), where *a*, *b*, and *c* first increased with an increasing temperature and again decreased to *a* = 6.8783(2) Å, *b* = 8.9831(2) Å, and *c* = 5.0478(2) Å when the sample was cooled, showing a reversible structural stability of the main phase. Two phases were used during the refinement of the diffraction of $NaFePO_4$/CNF electrodes: phase 1, $NaFePO_4$ (*Pmnb*); phase 2, $Na_3Fe(PO_4)_3$ (*R*3*c*). Fortunately, the $NaFePO_4$ lattice parameters in the $NaFePO_4$/CNF composites show minor changes without size broadening with *a* = 6.8671(2) Å, *b* = 8.9819(2) Å, and *c* = 5.0439(2) Å, which indicate that the structure of maricite $NaFePO_4$ was not affected during the high temperature procedures of carbon nanofiber formation.

3.2. Electrochemical Performance. To obtain fundamental knowledge of the electrochemical mechanism of the composite $NaFePO_4$/CNF cathode, it is important to study the contribution of each component to the total capacity. With a high carbon content, the electrochemical behavior of electrospun $NaFePO_4$/CNF may follow a different mechanism from a typical diffusion controlled intercalation material.[30] The energy storage mechanism of such materials can usually be divided into two parts: a charging process occurring at the surface of the material, which is referred to as the pseudocapacitive effect, and the sodium ion intercalation process along with redox reactions.[31] CV curves at different sweep rates can provide information on the surface controlled (capacitive) and diffusion controlled (bulk) processes.[32] Voltammetry at scan rates from 0.05 to 1 mV s^{-1} at a voltage window of 1.5−4.5 V were performed. From the CV curves shown in Figure 3a, a pair of broad redox peaks appear at 3.1 and 2.7 V, indicating the redox reaction of $Fe^{2+} \rightleftharpoons Fe^{3+} + e^-$. The capacitive effect in the system can be analyzed on the basis of the following equation:

$$i = av^b \tag{1}$$

where *i* is the current, ν is the scan rate, and *a* and *b* are adjustable parameters. In the well defined conditions, when *b* = 0.5, the current is diffusion controlled, indicating a faradaic intercalation process, while for *b* = 1, the current is surface controlled, indicating a capacitive process.[33] The *b* values as a function of potentials for $NaFePO_4$/CNF and pure CNF are shown in Figure 3b. We can see that, at 3.0 V, the *b* value for $NaFePO_4$/CNF is 0.75, while for CNF, the *b* value is 0.89. This indicates that, in $NaFePO_4$/CNF, the current originates partially from the Na^+ ion intercalation reaction other than the surface charging effect. Thus, the storage mechanism of electrospun $NaFePO_4$ is a mixed type with both diffusion and capacitive controlled contributions. The CV curves for the *b* value calculations of pure carbon nanofibers and cycled electrode are shown in Figure S4 of the Supporting Information.

In addition, a detailed examination of the voltammetry enables the quantitative calculation of the contribution of capacitive energy storage according to eq 2, with $k_1\nu$ and $k_2\nu^{0.5}$ corresponding to the current contributions from the capacitive surface effect and diffusion controlled intercalation process, respectively.[34] By determination of k_1 and k_2, one can quantify the fraction of the current from each contribution. As shown in panels c−e of Figure 3, the capacitive effects contribute to about 32.5, 49.9, and 60.0% at scan rates of 0.25, 0.5, and 1 mV s^{-1}, respectively. Hence, as expected, the capacitive effect becomes more dominant with an increasing scan rate.

$$|i_\nu| = k_1\nu + k_2\nu^{0.5}$$
$$|i_\nu|/\nu^{0.5} = k_1\nu^{0.5} + k_2 \tag{2}$$

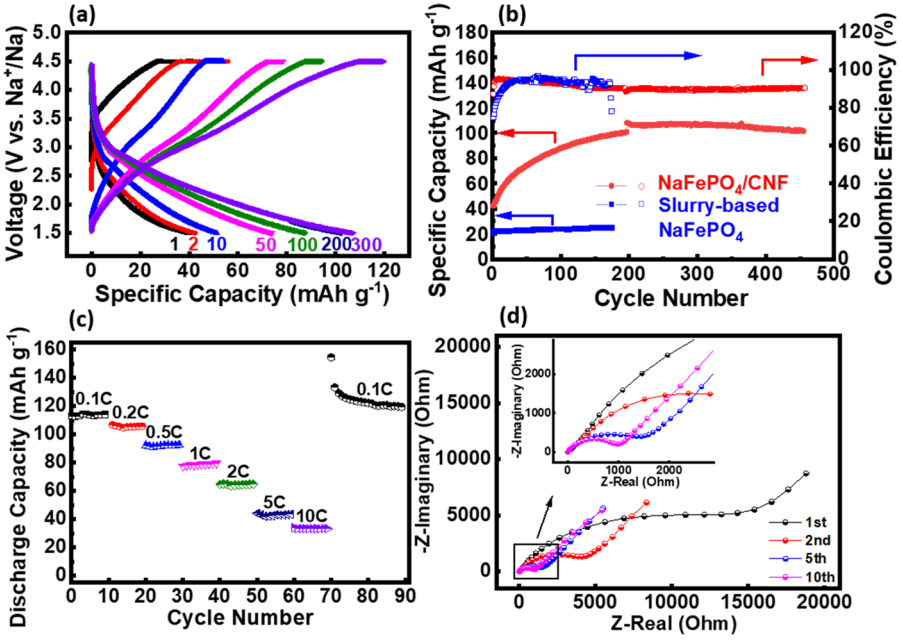

Figure 4. Electrochemical performance of the $NaFePO_4$/CNF electrodes: (a) charge–discharge curves at 0.1 C rate, (b) cycling stability with the comparison of slurry based $NaFePO_4$ at 0.1 C rate, (c) rate capability at different current rates, and (d) EIS of the $NaFePO_4$/CNF electrodes upon charge–discharge cycles.

The charge–discharge profiles of the electrospun electrodes are shown in Figure 4a at a C rate of 0.1 C between 1.5 and 4.5 V. Different from olivine $LiFePO_4$ and triphylite $NaFePO_4$, which have a voltage plateau from the first order phase transition, the sloping curve of maricite $NaFePO_4$ is indicative of a different sodium ion insertion/extraction mechanism, which probably results from solid solution behavior or a second order phase transition.[15] The specific discharge capacities are calculated on the basis of the mass of active material $NaFePO_4$, which is 30% of the full electrode weight. As seen, the discharge capacity is increasing from 42 mAh g^{-1} in the initial cycle up to 108 mAh g^{-1} in the 200th cycle, and then it is almost constant. Such an increasing capacity phenomenon was observed in many carbon containing cathode materials in SIBs.[7,35,36] Unfortunately, the observed increase of capacities during initial cycles lack possible suggestions and explanations. The following reasons for this increasing capacity phenomenon can be considered: (1) Carbon nanofibers break upon cycling, which generates more defects and storage sites for electrons. (2) With active material particles embedded in the carbon nanofibers, the mechanical breakdown of fibers increases contact between $NaFePO_4$ particles and the electrolyte, hence further facilitating the accessibility of these particles by ions.

To define the capacity contribution of carbon nanofibers, the electrochemical performance of the pure electrospun CNF carbonized at the same condition was also examined. Charge–discharge profiles of CNF (shown in Figure S5 of the Supporting Information) show a capacity of 22 mAh g^{-1} at 200 cycles with an initial discharge capacity of only 3 mAh g^{-1}. In comparison to the overall capacity of the hybrid cathode, the contribution from the non faradic reaction amounts to 20% after stabilization after 200 cycles. Other than electrospun $NaFePO_4$/CNF and pure CNF, a slurry made of $NaFePO_4$, Super P, and poly(vinylidene fluoride) (PVdF) with the same 30 wt % $NaFePO_4$ was also prepared and coated onto the surface of Al foil, labeled as slurry $NaFePO_4$. The long term performances of $NaFePO_4$/CNF and slurry $NaFePO_4$ are shown in Figure 4b with columbic efficiencies. After the initial increase in capacity, the $NaFePO_4$/CNF electrode reaches a capacity of 108 mAh g^{-1} after 200 cycles at 0.1 C (≈15 mA g^{-1}). In the following cycles, the electrode shows a good long term cycling stability with 94.4% retention after 450 cycles compared to the maximum value of 100% after 200 cycles. In comparison, a capacity of only 24 mAh g^{-1} was achieved for slurry $NaFePO_4$ and an irreversible capacity decay and cell failure occurred within 200 cycles, demonstrating that only the cell design of the composite of carbon nanofibers and maricite $NaFePO_4$ as a self standing electrode is able to deliver a stable long term electrochemical performance. The rate capability of the electrospun electrodes was also investigated (Figure 4c). Considering the increasing capacity in the first cycles, the electrode was cycled for over 150 cycles until the capacity reached a stable discharge specific capacity of 113.6 mAh g^{-1}. Afterward, different C rates were applied, delivering reversible capacities of 106.3 mAh g^{-1} at 0.2 C, 92.0 mAh g^{-1} at 0.5 C, 78.6 mAh g^{-1} at 1 C, 64.4 mAh g^{-1} at 2 C, 43.0 mAh g^{-1} at 5 C, and 33.3 mAh g^{-1} at 10 C. Importantly, when the cells were cycled back at 0.1 C afterward, a higher capacity with an average of 124.7 mAh g^{-1} was recovered, which indicates a good high rate capability and a reasonable tolerance of the rapid Na^+ ion insertion/extraction process. The specific capacity increased when the cell was brought back to 0.1 C from higher currents (124.7 mAh g^{-1}) compared to the first cycles at 0.1 C after the activation process (113.6 mAh g^{-1}). This may relate to an ongoing activating process, even during the high rate performance. Another possible explanation is that, at a higher C rate cycling, more electrons were quickly collected on the surface as a result of charge transfer.[37] Once the C rate went back to 0.1 C, the slower current allowed for a longer relaxation, which contributed to a higher capacity.

The electronic conductivity and its changes during cycling of the $NaFePO_4$/CNF electrode were analyzed by EIS. The Nyquist plots in Figure 4d consist of a semicircle in the high

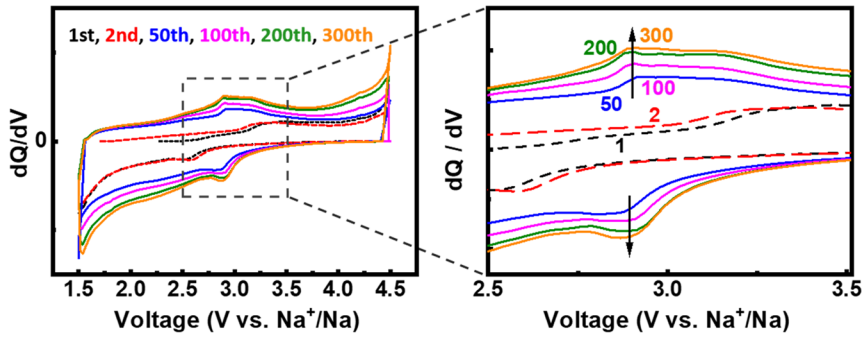

Figure 5. dQ/dV plots of $NaFePO_4$/CNF electrodes in the 1st, 2nd, 50th, 100th, 200th, and 300th cycles processed from galvanostatic charge–discharge curves.

frequency range, which is due to the ohmic resistance and charge transfer resistance, and a short inclined line in the low frequency range, which stems from the ionic diffusion within the electrodes.[38] The first parts of the semicircles from each cycle at high frequencies are overlapping, which can be caused by the solid electrolyte interface (SEI) formation within the first cycles. We can also observe that, in the Nyquist plots, the diameters of the semicircle of the electrodes decrease noticeably during cycling, which demonstrate that the charge transfer becomes faster and easier upon cycling within the first 10 cycles. The increasing conductivity also indicates an activation process of the electrodes upon charge–discharge. Furthermore, differential capacity diagrams (dQ/dV) shown in Figure 5 were plotted by processing the constant current charge–discharge data in the 1st, 2nd, 50th, 100th, 200th, and 300th cycles. In the initial cycles, no reduction/oxidation reaction peaks show up, indicative of a dominant capacitive behavior of the $NaFePO_4$/CNF electrode. Upon cycling, an increasing intensity of broad peaks at around 3 V can be observed, which agrees well with the gradual interaction of $NaFePO_4$ in the electrochemical behavior of the composite electrode, again confirming the gradual redox activation of Fe^{3+}/Fe^{2+} in $NaFePO_4$. Moreover, the separation of oxidation/reduction peaks is reduced in the first 100 cycles, indicating a reduced polarization.

3.3. *Ex Situ* and Activation Studies. The activation of $NaFePO_4$ in $NaFePO_4$/CNF electrodes was further confirmed by *ex situ* analysis of the samples after cycling. The Mössbauer spectra shown in Figure 6 demonstrate distinguished phases or sites in the respective samples. The intensities of Fe^{2+} and Fe^{3+} doublets were fitted to estimate the amount of each oxidation state in the samples of first cycle start, first cycle charged, first cycle discharged, 100th cycle start, 100th cycle charged, and 100th cycle discharged electrodes. While the as prepared $NaFePO_4$ powder shows exclusively Fe^{2+} after synthesis, some amount of Fe^{3+} is observed in the electrodes at the beginning of the first cycle and 100th cycle with an area fraction of 35.2 and 37.8%, respectively. This partial oxidation occurs during the stabilization process of the fiber mats, which is in agreement with the results from HT XRD, showing an impurity phase of oxidized Fe^{3+} in $Na_3Fe_2(PO_4)_3$. A rise in Fe^{2+} content from 35.2 to 43.2% appears during charging in the first cycle, while an increase from 37.8 to 63.0% is observed in the 100th cycle. After 100 cycles, more Fe^{3+} species exist at the charged state, which clearly demonstrates an increased $Fe^{3+/2+}$ activity upon extended cycling. This correlates with the results from Figure 3b, showing smaller b values of cycled $NaFePO_4$/CNF electrodes compared to those of non cycled

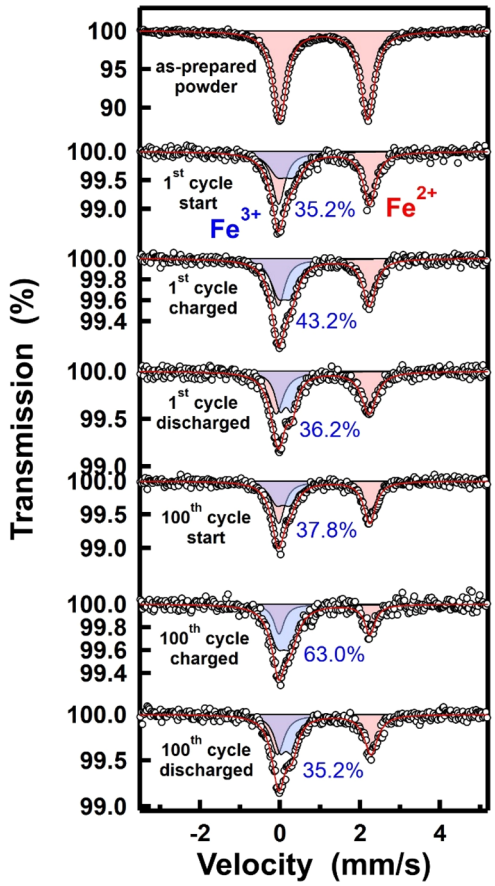

Figure 6. Fe Mössbauer spectra of as prepared $NaFePO_4$ powder and the $NaFePO_4$/CNF electrodes at charged and discharged states in the (top) 1st cycle and (bottom) 100th cycle. Experimental data points are shown as circles, with the overall fit as a red line, and the Fe^{2+} and Fe^{3+} sub spectra are shown as red and blue doublets, respectively.

$NaFePO_4$/CNF, demonstrating a more active $Fe^{2+} \rightleftharpoons Fe^{3+} + e^-$ redox reaction along cycling.

Raman spectra shown in Figure 7a illustrate the structural changes before and after cycling with fitted D and G bands of carbon. The ratio between I_D and I_G is often used as an indication of the degree of disorder/defects in carbonaceous materials.[39] In $NaFePO_4$/CNF, the intensity ratio of I_D/I_G decreased from 0.86 in the pristine state to 0.85 after 100 cycles. A significant structural change did not take place upon charge–discharge cycles, specifying a stable structure of the $NaFePO_4$/CNF electrode. The minor decrease of the I_D/I_G intensity correlates with the morphology observed by SEM in

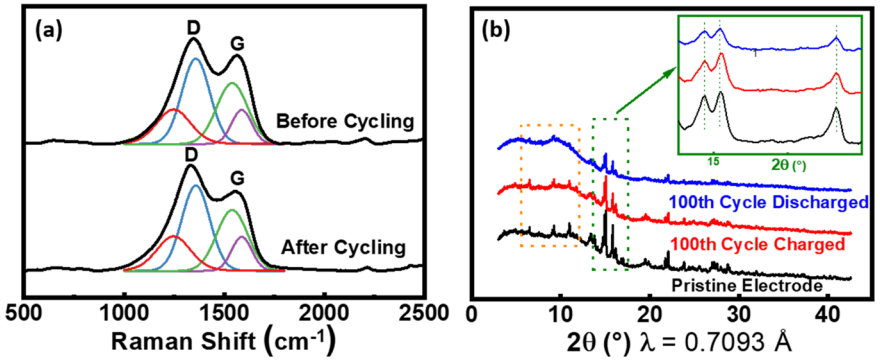

Figure 7. (a) Raman spectra of the $NaFePO_4$/CNF electrodes before and after cycling and (b) XRD patterns of the pristine and 100th cycled $NaFePO_4$/CNF electrodes.

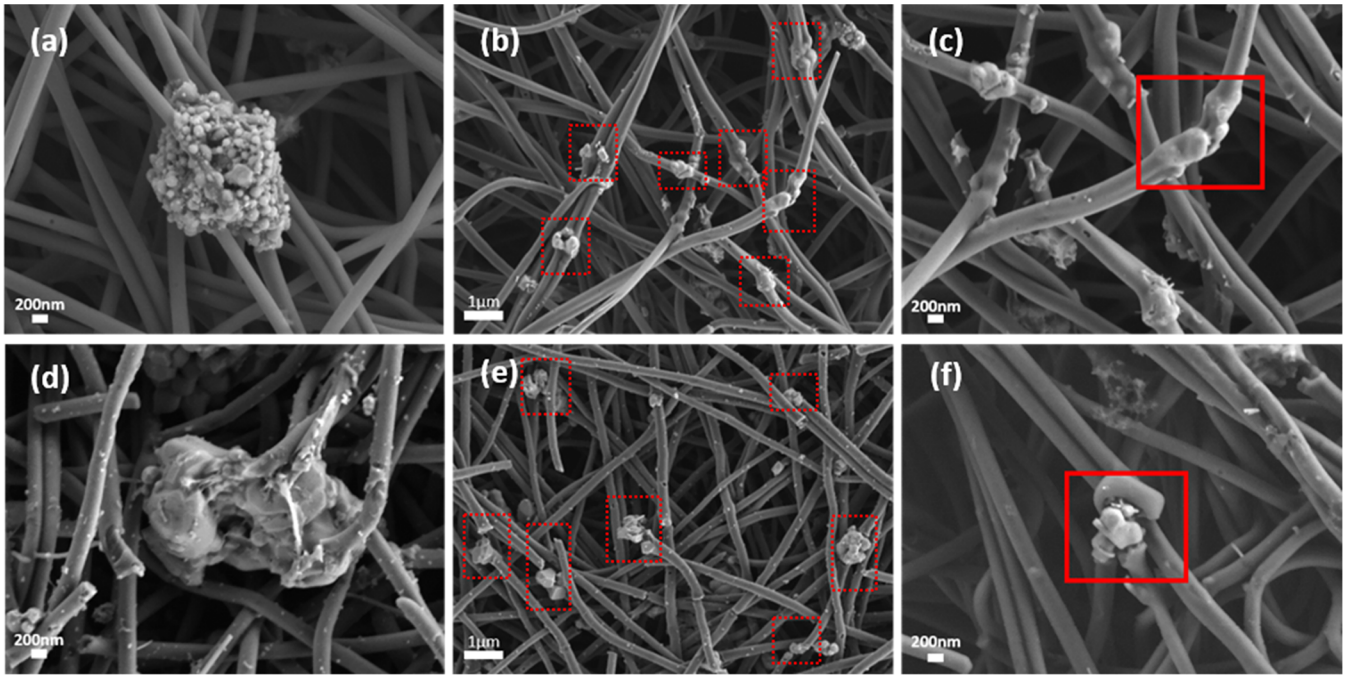

Figure 8. SEM pictures of (a–c) pristine electrodes and (d–f) intensely cycled $NaFePO_4$/CNF electrodes.

the cycled electrodes, as shown in Figure 8, with more cracks and partial defects allowing for more $NaFePO_4$ particles to become exposed and in contact with the electrolyte.

Moreover, more defects allow for more Na^+ ion transfer channels for an increased electrochemical performance. Furthermore, as seen from the SEM images, nanoparticle clusters with clear crystalline boundaries can be observed in pristine electrodes before cycling. However, after cycling, the sharp boundaries of the crystalline particles disappeared and transform to an agglomerated morphology. This further proves the involvement of $NaFePO_4$ particles in the electrochemical activity. Amorphous phases are observed in the XRD patterns of the samples charged and discharged in the 100th cycle, as shown in Figure 7b: areas marked with orange and green dashed rectangles include reflections with decreasing inten sities. By amplification of the reflections in the green marked area, we observe no shift of reflections in the cycled electrodes. A transformation of maricite $NaFePO_4$ into a completely amorphous phase has been observed from the XRD patterns of the electrodes charged up to 4.5 or 4.7 V.[14,16] In our $NaFePO_4$/CNF composite, the gradual activation of $NaFePO_4$ should theoretically lead to a gradual structural change. This perfectly explains the incomplete amorphization with retention of a high intensity of crystalline reflections in the electrodes after 100 cycles.

To further demonstrate the difference before and after intense cycling, STEM–EDX elemental mapping was carried out on pristine and intensively cycled electrodes. As shown in Figure 9, the nanofiber as the pristine electrode has a rather smooth surface, which shows no defects or cracks with the $NaFePO_4$ particles located on the surface. In comparison, a large crack appears on the fiber shown in panel b from an intensively cycled electrode, leaving the $NaFePO_4$ particles exposed. Moreover, some nanosized pores can also be observed on the surface of the intensively cycled electrode. By comparison of the electrodes before and after cycling, we were able to observe the gradual changes in the activity of $Fe^{2+} \rightleftharpoons Fe^{3+} + e^-$ redox reactions and the structures of both the carbon fiber and the maricite $NaFePO_4$ particles by various experimental methods. These *ex situ* results confirm an activation process of maricite $NaFePO_4$ involving the electro chemical behavior with slight mechanical breakdown and

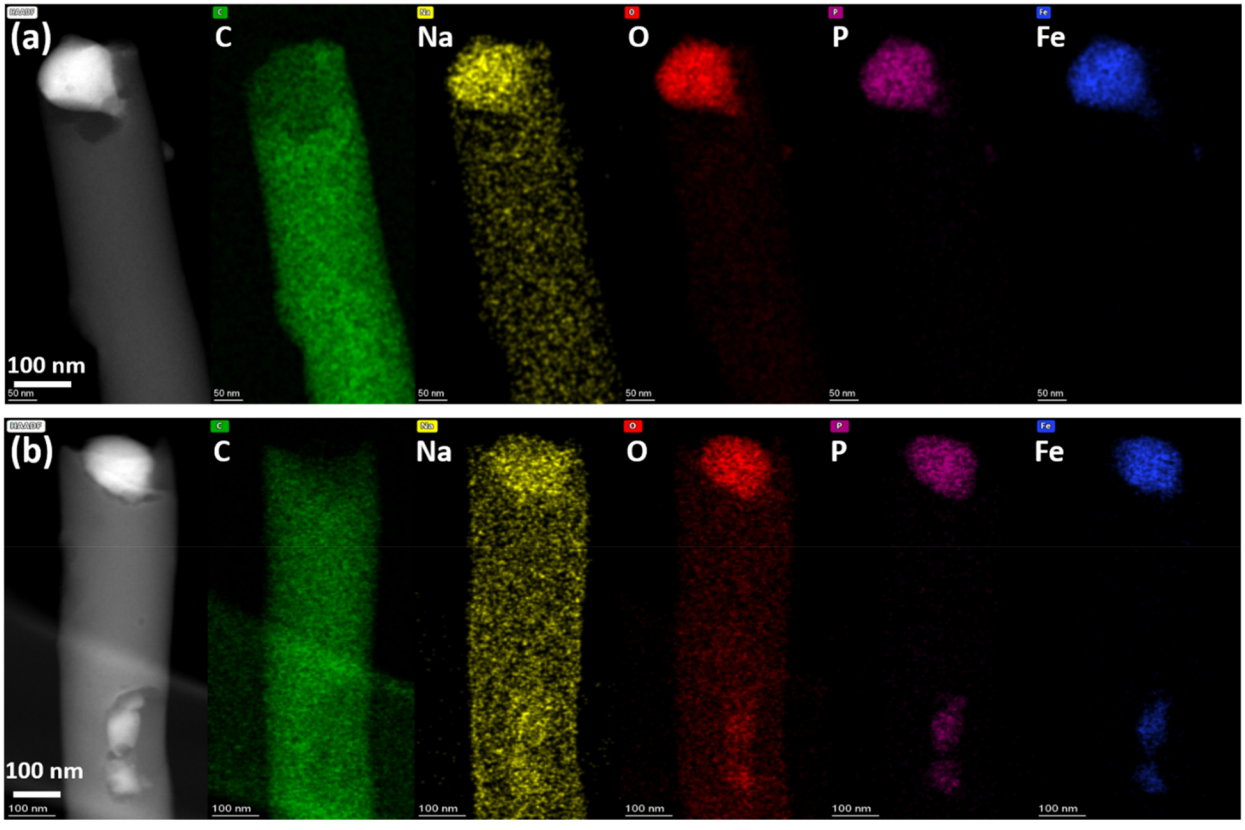

Figure 9. STEM−HAADF images of (a) pristine electrodes and (b) intensely cycled $NaFePO_4$/CNF electrodes.

defect formation of the carbon nanofibers. The activation process corresponds to an increased capacity appearing in the charge−discharge performance of $NaFePO_4$/CNF, which provides insight into the mechanism and the unique behavior of such self standing carbon integrated maricite $NaFePO_4$ electrodes.

4. CONCLUSION

Although maricite $NaFePO_4$ is considered as electrochemically inactive, the addition of an electrically conductive carbon nanofiber network results in a long term cycling stability of $NaFePO_4$. With the help of electrospinning, a self standing, collector free, and binder free maricite $NaFePO_4$/carbon nanofiber composite electrode was successfully prepared. A hybrid electrochemical mechanism of capacitive charge storage and intercalation based redox reaction of $Fe^{2+} \rightleftharpoons Fe^{3+} + e^-$ was confirmed by cyclic voltammograms at different scan rates. The phenomenon of an initially increasing capacity was explained along with *ex situ* measurements, demonstrating an activation process of $NaFePO_4$ particles in such composite electrodes. Even though a very high capacity was not delivered, this work presents a comprehensive study of such hybrid $NaFePO_4$ electrodes for the first time and enlightens the potential of self standing electrodes in future applications.

AUTHOR INFORMATION

Corresponding Author

Sylvio Indris − *Institute for Applied Materials (IAM), Karlsruhe Institute of Technology (KIT), 76344 Eggenstein Leopoldshafen, Germany;* orcid.org/0000 0002 5100 113X; Email: sylvio.indris@kit.edu

Authors

Xinyang Liu Théato − *Institute for Applied Materials (IAM), Karlsruhe Institute of Technology (KIT), 76344 Eggenstein Leopoldshafen, Germany*

Weibo Hua − *Institute for Applied Materials (IAM), Karlsruhe Institute of Technology (KIT), 76344 Eggenstein Leopoldshafen, Germany;* orcid.org/0000 0001 5372 4422

Hang Li − *Institute for Applied Materials (IAM), Karlsruhe Institute of Technology (KIT), 76344 Eggenstein Leopoldshafen, Germany*

Michael Knapp − *Institute for Applied Materials (IAM), Karlsruhe Institute of Technology (KIT), 76344 Eggenstein Leopoldshafen, Germany*

Georgian Melinte − *Institute of Nanotechnology (INT), Karlsruhe Institute of Technology (KIT), 76344 Eggenstein Leopoldshafen, Germany*

Helmut Ehrenberg − *Institute for Applied Materials (IAM), Karlsruhe Institute of Technology (KIT), 76344 Eggenstein Leopoldshafen, Germany;* orcid.org/0000 0002 5134 7130

Complete contact information is available at:

Notes

The authors declare no competing financial interest.

■ ACKNOWLEDGMENTS

The authors thank Dr. Nicola P. M. Casati and Dr. Manuel Wilke from PSI, Switzerland, for their kind support in the synchrotron XRD measurement. This work contributes to the research performed at the Center for Electrochemical Energy Storage Ulm Karlsruhe (CELEST) and was funded by the German Research Foundation (DFG) under Project 390874152 (POLiS Cluster of Excellence).

■ REFERENCES

(1) Slater, M. D.; Kim, D.; Lee, E.; Johnson, C. S. Sodium Ion Batteries. *Adv. Funct. Mater.* **2013**, *23*, 947−958.

(2) Palomares, V.; Serras, P.; Villaluenga, I.; Hueso, K. B.; Carretero González, Y.; Rojo, T. Na Ion Batteries, Recent Advances and Present Challenges to Become Low Cost. *Energy Environ. Sci.* **2012**, *5*, 5884−5901.

(3) Hwang, J. Y.; Myung, S. T.; Sun, Y. K. Sodium Ion Batteries: Present and Future. *Chem. Soc. Rev.* **2017**, *46*, 3529−3614.

(4) Kim, S. W.; Seo, D. H.; Ma, X.; Ceder, G.; Kang, K. Electrode Materials for Rechargeable Sodium Ion Batteries: Potential Alter natives to Current Lithium Ion Batteries. *Adv. Energy Mater.* **2012**, *2*, 710−721.

(5) Yuan, L. X.; Wang, Z. H.; Zhang, W. X.; Hu, X. L.; Chen, J. T.; Huang, Y. H.; Goodenough, J. B. Development and Challenges of $LiFePO_4$ Cathode Material for Lithium Ion Batteries. *Energy Environ. Sci.* **2011**, *4*, 269−284.

(6) Xu, G. L.; Amine, R.; Abouimrane, A.; Che, H.; Dahbi, M.; Ma, Z. F.; Saadoune, I.; Alami, J.; Mattis, W. L.; Pan, F.; Chen, Z.; Amine, K. Challenges in Developing Electrodes, Electrolytes, and Diagnostics Tools to Understand and Advance Sodium Ion Batteries. *Adv. Energy Mater.* **2018**, *8*, 1702403.

(7) Fang, Y.; Liu, Q.; Xiao, L.; Ai, X.; Yang, H.; Cao, Y. High Performance Olivine $NaFePO_4$ Microsphere Cathode Synthesized by Aqueous Electrochemical Displacement Method for Sodium Ion Batteries. *ACS Appl. Mater. Interfaces* **2015**, *7*, 17977−17984.

(8) Oh, S. M.; Myung, S. T.; Hassoun, J.; Scrosati, B.; Sun, Y. K. Reversible $NaFePO_4$ Electrode for Sodium Secondary Batteries. *Electrochem. Commun.* **2012**, *22*, 149−152.

(9) Burba, C. M.; Frech, R. Vibrational Spectroscopic Investigation of Structurally Related $LiFePO_4$, $NaFePO_4$, and $FePO_4$ Compounds. *Spectrochim. Acta, Part A* **2006**, *65*, 44−50.

(10) Casas Cabanas, M.; Roddatis, V. V.; Saurel, D.; Kubiak, P.; Carretero González, J.; Palomares, V.; Serras, P.; Rojo, T. Crystal Chemistry of Na Insertion/deinsertion in $FePO_4$ $NaFePO_4$. *J. Mater. Chem.* **2012**, *22*, 17421−17423.

(11) Lepage, Y.; Donnay, G. The Crystal Structure of the New Mineral Maricite, $NaFePO_4$. *Can. Mineral.* **1977**, *15*, 518−521.

(12) Li, J.; Ma, Z. F. Past and Present of $LiFePO_4$: From Fundamental Research to Industrial Applications. *Chem.* **2019**, *5*, 3−6.

(13) Xiong, F.; An, Q.; Xia, L.; Zhao, Y.; Mai, L.; Tao, H.; Yue, Y. Revealing the Atomistic Origin of the Disorder Enhanced Na Storage Performance in $NaFePO_4$ Battery Cathode. *Nano Energy* **2019**, *57*, 608−615.

(14) Kim, J.; Seo, D. H.; Kim, H.; Park, I.; Yoo, J. K.; Jung, S. K.; Park, Y. U.; Goddard, W. a.; Kang, K. Unexpected Discovery of Low Cost Maricite $NaFePO_4$ as a High Performance Electrode for Na Ion Batteries. *Energy Environ. Sci.* **2015**, *8*, 540−545.

(15) Rahman, M. M.; Sultana, I.; Mateti, S.; Liu, J.; Sharma, N.; Chen, Y. Maricite $NaFePO_4$/C/graphene: A Novel Hybrid Cathode for Sodium Ion Batteries. *J. Mater. Chem. A* **2017**, *5*, 16616−16621.

(16) Liu, Y.; Zhang, N.; Wang, F.; Liu, X.; Jiao, L.; Fan, L. Z. Approaching the Downsizing Limit of Maricite $NaFePO_4$ toward High Performance Cathode for Sodium Ion Batteries. *Adv. Funct. Mater.* **2018**, *28*, 1801917.

(17) Coffey, B.; Madsen, P. V.; Poehler, T. O.; Searson, P. C. High Charge Density Conducting Polymer/Graphite Fiber Composite Electrodes for Battery Applications. *J. Electrochem. Soc.* **1995**, *142*, 321.

(18) Zhang, X.; Ji, L.; Toprakci, O.; Liang, Y.; Alcoutlabi, M. Electrospun Nanofiber Based Anodes, Cathodes, and Separators for Advanced Lithium Ion Batteries. *Polym. Rev.* **2011**, *51*, 239−264.

(19) Wang, H. G.; Yuan, S.; Ma, D. L.; Zhang, X. B.; Yan, J. M. Electrospun Materials for Lithium and Sodium Rechargeable Batteries: From Structure Evolution to Electrochemical Performance. *Energy Environ. Sci.* **2015**, *8*, 1660−1681.

(20) Zhu, Y.; Han, X.; Xu, Y.; Liu, Y.; Zheng, S.; Xu, K.; Hu, L.; Wang, C. Electrospun Sb/C Fibers for a Stable and Fast Sodium Ion Battery Anode. *ACS Nano* **2013**, *7*, 6378−6386.

(21) Liu, J.; Tang, K.; Song, K.; Van Aken, P. a.; Yu, Y.; Maier, J. Electrospun $Na_3V_2(PO_4)_3$/C Nanofibers as Stable Cathode Materials for Sodium Ion Batteries. *Nanoscale* **2014**, *6*, 5081−5086.

(22) Liu, Y.; Huang, K.; Fan, Y.; Zhang, Q.; Sun, F.; Gao, T.; Wang, Z.; Zhong, J. Binder Free Si Nanoparticles@carbon Nanofiber Fabric as Energy Storage Material. *Electrochim. Acta* **2013**, *102*, 246−251.

(23) Bachtin, K.; Kramer, D.; Chakravadhanula, V. S. K.; Mu, X.; Trouillet, V.; Kaus, M.; Indris, S.; Ehrenberg, H.; Roth, C. Activation and Degradation of Electrospun $LiFePO_4$ Battery Cathodes. *J. Power Sources* **2018**, *396*, 386−394.

(24) Bachtin, K.; Kaus, M.; Pfaffmann, L.; Indris, S.; Knapp, M.; Roth, C.; Ehrenberg, H. Comparison of Electrospun and Conven tional $LiFePO_4$/C Composite Cathodes for Li Ion Batteries. *Mater. Sci. Eng., B* **2016**, *213*, 98−104.

(25) Hou, H.; Qiu, X.; Wei, W.; Zhang, Y.; Ji, X. Carbon Anode Materials for Advanced Sodium Ion Batteries. *Adv. Energy Mater.* **2017**, *7*, 1602898.

(26) Avdeev, M.; Mohamed, Z.; Ling, C. D.; Lu, J.; Tamaru, M.; Yamada, A.; Barpanda, P. Magnetic Structures of $NaFePO_4$ Maricite and Triphylite Polymorphs for Sodium Ion Batteries. *Inorg. Chem.* **2013**, *52*, 8685−8693.

(27) Wang, D.; Wu, Y.; Lv, J.; Wang, R.; Xu, S. Carbon Encapsulated Maricite $NaFePO_4$ Nanoparticles as Cathode Material for Sodium Ion Batteries. *Colloids Surf., A* **2019**, *583*, 123957.

(28) Kosova, N. V.; Podugolnikov, V. R.; Devyatkina, E. T.; Slobodyuk, A. B. Structure and Electrochemistry of $NaFePO_4$ and Na_2FePO_4F Cathode Materials Prepared via Mechanochemical Route. *Mater. Res. Bull.* **2014**, *60*, 849−857.

(29) Sun, A.; Beck, F. R.; Haynes, D.; Poston, J. A.; Narayanan, S. R.; Kumta, P. N.; Manivannan, A. Synthesis, Characterization, and Electrochemical Studies of Chemically Synthesized $NaFePO_4$. *Mater. Sci. Eng., B* **2012**, *177*, 1729−1733.

(30) Gogotsi, Y.; Penner, R. M. Energy Storage in Nanomaterials—Capacitive, Pseudocapacitive, or Battery Like? *ACS Nano* **2018**, *12*, 2081−2083.

(31) Wang, J.; Polleux, J.; Lim, J.; Dunn, B. Pseudocapacitive Contributions to Electrochemical Energy Storage in TiO_2 (anatase) Nanoparticles. *J. Phys. Chem. C* **2007**, *111*, 14925−14931.

(32) Tian, G.; Zhao, Z.; Sarapulova, A.; Das, C.; Zhu, L.; Liu, S.; Missiul, A.; Welter, E.; Maibach, J.; Dsoke, S. Understanding the Li Ion Storage Mechanism in a Carbon Composited Zinc Sulfide Electrode. *J. Mater. Chem. A* **2019**, *7*, 15640−15653.

(33) Bard, A. J.; Faulkner, L. R. *Electrochemical Methods: Fundamentals and Applications*; Harris, D., Ed.; John Wiley & Sons: New York, 1980; pp 161−176.

(34) Ma, Y.; Ma, Y.; Bresser, D.; Ji, Y.; Geiger, D.; Kaiser, U.; Streb, C.; Varzi, A.; Passerini, S. Cobalt Disulfide Nanoparticles Embedded in Porous Carbonaceous Micro Polyhedrons Interlinked by Carbon Nanotubes for Superior Lithium and Sodium Storage. *ACS Nano* **2018**, *12*, 7220−7231.

(35) Wang, D.; Wu, Y.; Lv, J.; Wang, R.; Xu, S. Carbon Encapsulated Maricite $NaFePO_4$ Nanoparticles as Cathode Material for Sodium Ion Batteries. *Colloids Surf., A* **2019**, *583*, 123957.
(36) Jin, T.; Liu, Y.; Li, Y.; Cao, K.; Wang, X.; Jiao, L. Electrospun $NaVPO_4F$/C Nanofibers as Self Standing Cathode Material for Ultralong Cycle Life Na Ion Batteries. *Adv. Energy Mater.* **2017**, *7*, 1700087.
(37) Vlad, A.; Singh, N.; Rolland, J.; Melinte, S.; Ajayan, P. M.; Gohy, J. F. Hybrid Supercapacitor Battery Materials for Fast Electrochemical Charge Storage. *Sci. Rep.* **2015**, *4*, 4315.
(38) Zhu, Y.; Xu, Y.; Liu, Y.; Luo, C.; Wang, C. Comparison of Electrochemical Performances of Olivine $NaFePO_4$ in Sodium Ion Batteries and Olivine $LiFePO_4$ in Lithium Ion Batteries. *Nanoscale* **2013**, *5*, 780−787.
(39) Ferrari, A. C.; Robertson, J. Interpretation of Raman Spectra of Disordered and Amorphous Carbon. *Phys. Rev. B: Condens. Matter Mater. Phys.* **2000**, *61*, 14095−14107.